Optimization of Microfluidic Tools for Serial Femtosecond Crystallography with X-ray Free Electron Lasers via 3D-Printing

Subtopic:
Material Science

Final Report

Author:
Naderer Christoph
Master's program Medical Engineering
At the University of applied Science Upper Austria
School of Applied Health and Social Sciences
Garnisonstraße 21, 4020 Linz, Austria

Date of Submission:
Linz, on the 30th of April 2020

Academic Advisors:
FH-Prof. DI Dr. Jaroslaw Jacak
University of Applied Science Upper Austria,
Department of Medical Engineering

Prof. Alexandra Ros, PhD Habil.
Associate Professor, School of Molecular Sciences
Biodesign Center for Applied Structural Discovery
Arizona State University

Table of Contents

1 Initial Situation / Problem

Polymers are used in a broad field of research. Especially, in microfluidics the composition of monomers is of great importance to alter the function of the polymer device. Microfluidics themselves are used in life science, fluid dynamics or bio power generation. [1] Recent developments established microfluidics for applications in crystallography. Protein crystallography with high energy x-ray sources such as free electron lasers (XFELs) has become an emerging technique for structure elucidation of complex proteins. [2], [3] This approach to analyze the structure of proteins requires certain injection approaches as one crystal at a time (serial crystallography, SC) interacts with a fs-long laser pulse providing a unique diffraction pattern representing a certain protein. [4] As the delivery of one protein crystal at the time is required to obtain significant data it is of great importance to alter the surface within the device to increase the outcome of significant data. One major problem in the delivery of proteins in a microfluidic device is clogging. Clogging occurs as proteins adsorb to the inner surface of the delivering device leading to a pressure build up and eventual rupture of the device. [5] The destruction of the device leads to an obvious loss of sample and precious time at XFEL facilities for crystallography experiments. The protein binding properties of current microfluidic have been observed as highly nonspecific and tricky to modify. Polyethylene glycols (PEG) are known to modify the protein binding properties of acrylate structures. [6] Unfortunately, there is currently no approach to use PEGs in the production of microfluidic devices for sample delivery at protein crystallography experiments. Besides the problem of clogging sample wastage remains a problem. Only a small amount of proteins in solution provides diffraction patterns as a continuous stream is delivered to the XFEL. Therefore, the continuous stream towards the XFEL has been improved to droplet delivery of droplets of nL to pL . [7] For such droplet delivery the surface of the device requires certain properties regarding wettability. Besides electrical triggering for the droplet to synchronize the sample delivery with the XFEL pulse train it is required to establish a co-flow of an aqueous and an oil phase inside the microfluidic device. [8] To increase the reliability for establishing the co-flow hydrophobic surface properties inside the device would enhance the flow conditions. Fluorinated acrylates are known to show highly hydrophobic properties [9] but have not been used as UV-curable systems for coatings inside of microfluidic devices.

This research report presents the development of a protocol to use a PEG acrylate to modify the protein binding properties of an acrylate structure in 2D and 3D printed with the Nanoscribe Lithography setup available at Arizona State University and the development of a hydrophobic surface coating for acrylate structures via UV-crosslinking.

In the future these protocols can be used to produce microfluidic devices for protein crystallography experiments with certain surface properties. These properties can be introduced to increase the hydrophobicity in certain areas of the device and reduce the probability of clogging by reducing the unspecific binding of proteins. The application in microfluidic devices is not part of this report.

1.1 Introduction Lithography

Optical lithography describes the process of forming patterns of photosensitive polymers (photoresist) on a substrate. [10] Optical lithography can be distinguished into mask patterning and mask free lithography (e.g. direct laser writing). For mask patterning the pattern of a photomask is transferred via exposure of the photoresist through a photomask to UV-light. First the photoresist is coated onto the substrate. In a second step the photoresist is exposed to UV light and a photomask is used to imprint the desired pattern. The substrate is submerged in a developing agent and depending on the photoresist the exposed (positive photoresist) or the unexposed (negative photoresist) areas are dissolved. Afterwards etching is used to transfer the pattern onto the substrate. Finally, the photoresist is stripped of or dissolved. (Figure 1). [11]

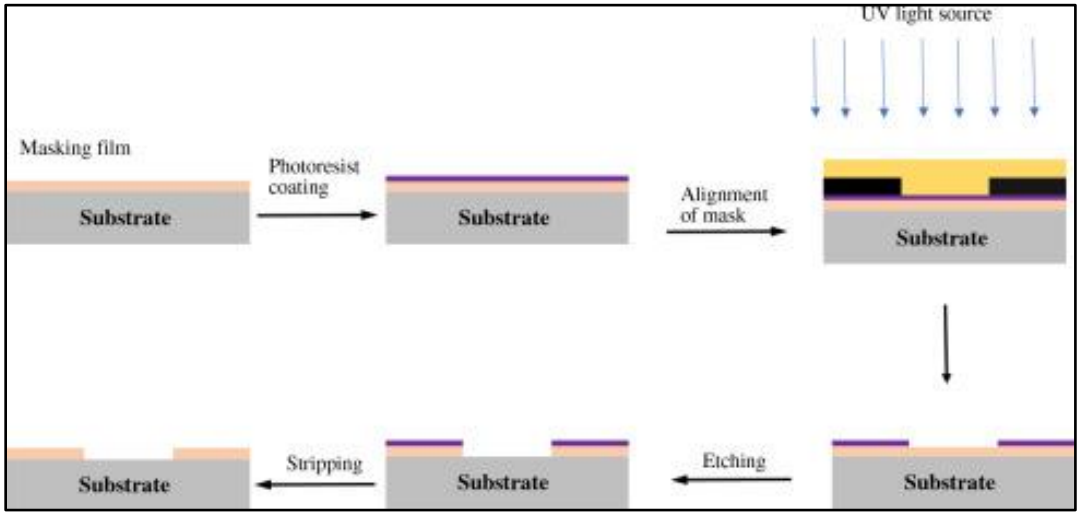

Figure 1 Optical lithography process: First the substrate is coated with the photoresist. A photomask is used to transfer a pattern via UV-exposure. Depending on the photoresist the exposed (positive photoresist) or the unexposed (negative photoresist) areas are dissolved as the substrate is submerged in a developing agent. Etching is used to transfer the pattern onto the substrate. In a final step the remaining photoresist is stripped of or dissolved. [11]

Mask free lithography or direct laser writing (DLW) uses ultra-fast laser beams (most commonly wavelengths in the near infrared range, high intensity, and pulse lengths down to femtoseconds) to start the polymerization in a small volume (voxel). Resolutions below 100nm have been achieved using this technique (Figure 2). [12] Using optical enhancements like Stimulated emission depletion or two photon absorption (Multi photon lithography MPL) the resolution can be further enhanced. [13] The pattern of writing can be chosen freely allowing for any arbitrary structure desired. This technique allows for 2D and 3D applications alike. Acrylate monomers are well suited for MPL, as they are highly reactive allowing for high writing speed and are transparent in the visual spectral regime.[13], [14] A typical monomer for MPL is Pentaerythritol triacrylate (PETA). This monomer is well suited for this project as it furthermore provides high optical stability, which is required as the microfluidic devices are exposed to high energy lasers for positioning during XFEL experiments. To start the polymerization a photoinitiator is needed. A photoinitiator is a type of molecule which releases radicals in the process of getting excited by absorption of photons at a certain wavelength and relaxation afterwards. [15] Irgacure 819 was chosen for this project due to the low autofluorescence it provides.

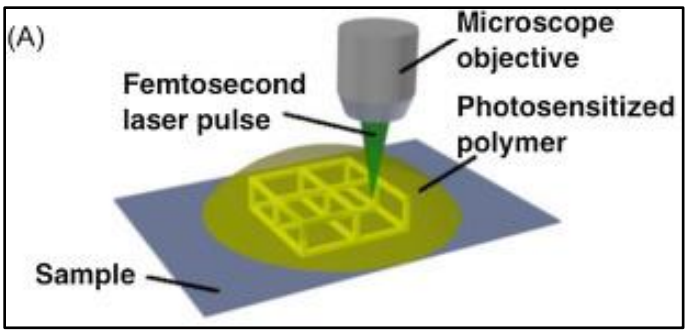

Figure 2 Direct laser writing uses high frequency and intensity laser pulses in the near infrared range to polymerize small volumes (voxel). Mirrors guiding the laser beam within the photosensitized polymer allow any desired pattern as the voxel pattern is fabricated directly by the laser and no mask pattern is needed. This technique allows to generate structures at a resolution sub 100nm. [12] The laser is focused inside a photosensitized polymer consisting of a monomer and a photoinitiator. A photoinitiator forms reactive species (e.g. radicals) upon relaxation out of the excited state when irradiated at a certain wavelength starting the polymerization. [15]

1.2 Surface properties

A surface defines the outer atomic layer of a solid object in contact with the environment. Depending on the composition of this layer the solid shows certain properties. Surface properties include structure, surface energy, surface charge, adhesion and adsorption properties. [16]

1.2.1 Wettability

Wettability describes the ability of a solid surface to maintain contact with a liquid and is mainly dependent on the surface energy. [17] The surface energy of the liquid, the solid and the surrounding gas allow to calculate the contact angle of a liquid droplet on the surface of the solid (Figure 3a). [18] Depending on the contact angle the surface is defined as hydrophilic or hydrophobic. Hydrophobic surfaces are considered surfaces presenting a contact angle of 90 degrees or higher while contact angles below 90 degrees are reckoned as hydrophilic surfaces (Figure 3b,c). [19] The design of either hydrophilic or hydrophobic areas in a channel has a huge impact on the flow and the capillary function within the channel of a microfluidic device. [20] Providing a hydrophobic surface within a microfluidic channel enables the device to generate a co-flow of an oil phase with droplets of an aqueous solution and can be used to deliver droplets containing one protein at a time in XFEL experiments. [8]

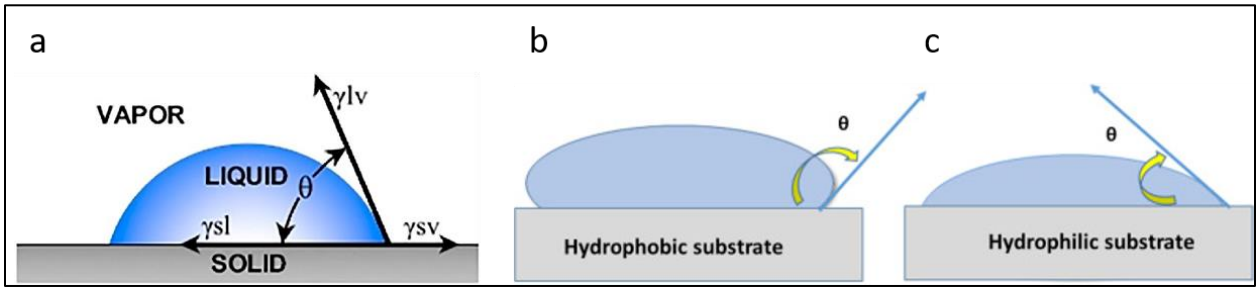

Figure 3 (a) The surface energy of the solid and the interaction of the surface energy between the solid and the liquid as well as the sold and vapor and the liquid and the vapor define the contact angle of a liquid droplet on a solid surface. [18] Depending on the composition of the solid material the material is either hydrophobic(b) or hydrophobic (c). Hydrophobic surfaces are considered surfaces presenting a contact angle of more than 90 degrees. Hydrophilic surfaces however show contact angles below 90 degrees. [19]

1.2.2 Protein binding

Protein binding can be differentiated into two groups, specific protein binding and nonspecific protein binding. Typically, proteins tend to bind to a specific protein counterpart as the protein itself offers binding sites which allow only the binding of the counterpart (e.g. biotin streptavidin). This interaction is well known and has been used to investigate the binding of proteins on various surfaces. [21]–[23]. Nonspecific binding occurs as proteins bind to anything besides their designated counterpart. [24] The nonspecific binding is random and typically undesired in biological and biophysical experiments as it increases background noise or hinders the target protein from binding. [25] Even the loss of function of optical elements has been observed as a layer of nonspecific bound proteins accumulates over time. [26] Not only is the nonspecific binding of proteins on polymeric structures problematic as it can lead to clogging of the device but the adsorption and desorption of proteins on a solid surface is usually a reversible process. The desorption of proteins can lead to the problem of an alteration within the protein structure. [27] The altered protein structure can be problematic especially in crystallography experiments where highly purified samples over a long period of experiments is required to generate significant data.

2 Methods / Evaluation

The challenges of this project have been tackled using several approaches and techniques to generate polymeric 2D and 3D structures and to evaluate the contact angle of the structures as well as the protein bind properties of the structures.

2.1 Material

To meet the requirements regarding resolution, fast writing speed and transparency in the visible spectrum Pentaerythritol triacrylate (PETA) (structure Figure 4) was chosen as acrylate to establish the protocols to write 2D and 3D structures. [13] PETA is commercially available and is versatile in the application for 3D printing and the production of microfluidic devices.

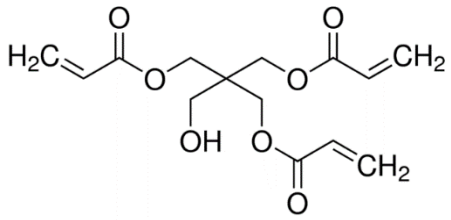

Figure 4 Chemical structure of Pentaerythritol triacrylate (PETA). [28]

Polyethylene glycols (PEG) are known to reduce the nonspecific bindings of proteins by a margin. [6] To incorporate the binding properties of PEG in an acrylate structure Polyethylene glycol diacrylate (PEGDA) (structure Figure 5) is a common approach. [29] PEGDA can be mixed conveniently with other acrylates and was chosen to modify the binding properties of the main acrylate PETA.

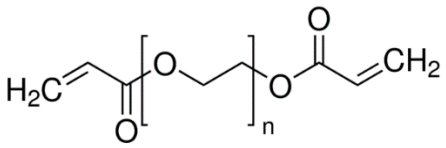

Figure 5 Chemical structure of Polyethylene glycol diacrylate (PEGDA). [30]

Surfaces consisting of fluorinated molecules show low surface energy and thus yielding a high contact angle. [31] To establish a protocol to bind a fluorine group to an acrylate structure via UV-crosslinking a fluorinated acrylate has been chosen. Fluorinated acrylates have been developed in the past to generate hydrophobic surfaces but were not used to coat existing acrylate structures. [9] 2,2,3,3,4,4,5,5,6,6,7,7-Dodecafluoroheptyl acrylate (DFHA) (structure Figure 6) has been chosen as the acrylate provides a long fluorine group and the acrylate group will be used to crosslink the DFHA to unpolymerized residuals on the surface of the PETA structures.

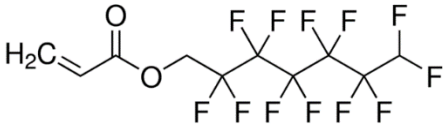

Figure 6 Chemical structure of 2,2,3,3,4,4,5,5,6,6,7,7-Dodecafluoroheptyl acrylate (DFHA). [32]

Autofluorescence can be a challenging problem in the application of 3D printed polymer structures. Residuals of the used photoinitiator causes the structure to generate an undesired high background signal. Phenylbis(2,4,6-trimethylbenzoyl)phosphine oxide (Irgacure 819) (structure Figure 7)is known to show low autofluorescence, allow fast writing speed up to cm/s and high resolution. [13], [14]

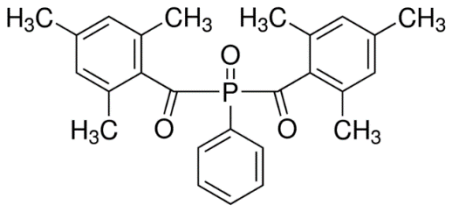

Figure 7 Chemical structure of Phenylbis(2,4,6-trimethylbenzoyl)phosphine oxide (Irgacure 819). [33]

2.2 Spin coating

Spin coating is a process to form a homogenous surface of a photoresist on a substrate. This is accomplished by rapidly spinning the substrate while dispensing portions of the polymer on the surface. Surface tension of the liquid polymer, spin speed, acceleration and spin time determine the film thickness after the process. Depending on the viscosity of the polymer the parameters need to be adjusted accordingly. [34]

2.3 UV-curable coating

Polymers are often used to alter the surface properties of many different substrates. [35] Acrylates in general are well known for their fast curing at UV exposure. [36] Therefore, photoresists containing acrylates are often used as coatings. PETA is well known to perform well as a crosslinking agent between acrylate polymers. [37] The acrylate residuals at the surface can easily crosslink with acrylates presented

in a coating and exposure to UV-light. The time required for curing the photoresist depends on the acrylate and the amount of photoinitiator. Higher polymerization is achieved by higher UV-light intensity, longer exposure times or addition of a co-photoinitiator.

2.4 Nanoscribe 3D printer

The Nanoscribe system Photonic Professional GT is a commercially available 3D printing system providing resolutions down to 200nm and writing speed up to several cm/s while allowing to print structures bigger than 100 µm. The system relies on MPL at 780nm and fs-excitation in a Dip-in laser lithography setup (DiLL). [38] The system is built as an inverted microscope to observe the printing process with an implemented optical pathway for the laser to write the structure.
To produce structures using the system a toolchain has to be operated. First, the device needs to be designed using a 3D design software. Secondly the design needs to be transformed into a .stl-file. The .stl-file is translated using Describe, a software provide by the company Nanoscribe to produce the code the 3D printer can operate. Finally. the code itself needs to be adjusted for the used photoresist. The 3D printing process is fully automated once the system is provided with the sample inside the system and the code.

2.4.1 Model

To design the test structures for the surface coating and the protein binding in 2D two simple designs have been chosen. For the coating tests a simple block of 5x5 mm and a height of 50 µm and for the protein binding tests a grid of 1x1 mm and a grid constant of 25 µm was constructed in Fusion360. Fusion360 conveniently provides the possibility to directly export the design as .stl-file.

2.4.2 Code

The code was generated using Describe. This software allows to split the design into blocks which represent the working range of the galvanometer mirrors in the 3D printer guiding the laser. Besides the working range the slice thickness and the hatching thickness are adjusted. Slice thickness represents the jumps lateral and the hatching distance allows to set the distance axial describing the path of the laser. In the code the laser power and the writing speed can be adjusted. The laser power is adjusted via providing a scaling percentage of the maximum laser power. [39] To decrease the time required for the printing the path of the laser can be adjusted but this adjustments lead to a reduction in stability of the structure.

2.4.3 Sample preparation and development

The photoresist was mixed using an ultrasonication bath to dissolve the photoinitiator in the monomer. The amount of monomer and photoinitiator were weighed in using a high precision scale. The mixture was sonicated for 2-3h until the photoinitiator was completely dissolved.
The glass slides for the Nanoscribe setup are reusable ITO-coated (Indium Tin Oxide) glass slides. Before each printing procedure, the glass slides are cleaned using Acetone and Isopropanol.
A droplet of photoresist was applied to the surface of the ITO-glass slide and inserted into the Nanoscribe system to start the 3D printing process. An Auto-Focus function is used to find the surface of the ITO-glass slide.
After the printing process the sample was developed in SU-8 developer for 5 minutes and rinsed with Isopropanol to wash away any excess SU-8 developer.

2.5 Contact angle measurement

To measure the hydrophobicity of a surface one approach is to measure the contact angle. To measure the contact angle one possibility is to apply a droplet of water to the surface and measure the angle between the droplet and the solid surface. The image of the droplet was taken with a microscope setup seen in Figure 8.

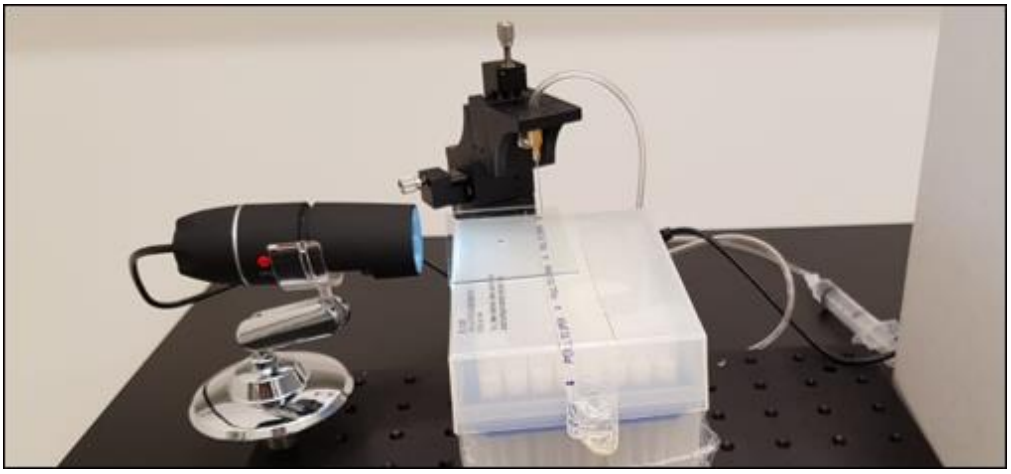

Figure 8 Microscope setup to image water droplets on polymer surfaces. The droplet of water is applied using a pipette.

To calculate the contact angle a toolbox of ImageJ was used. This toolbox allows to estimate the angle at the edge of the droplet by fitting a circle or an ellipse to the shape of the droplet. A tangent is fitted at endpoints of the droplet. (Figure 9b). The circle or ellipse is fitted to 5 points which are chosen by user input. The top of the droplet, both ends and two points along the edge on each side between top and bottom of the droplet are required (Figure 9a). The contact angle is calculated by subtracting the value provided by the program from 180 degrees. The contact angle was measured on multiple samples. To visualize the difference in contact angle across the used photoresist a boxplot was generated using a Python script. Mean values and the standard deviation for the contact angle have been calculated as well.

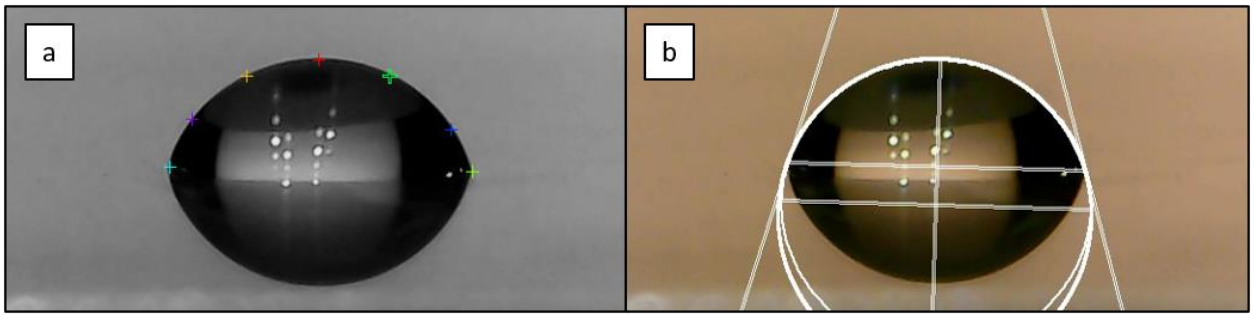

Figure 9 Contact angle determination using an ImageJ toolbox. (a) 5 points along the edge of the water droplet are selected by user input to fit a circle or an ellipse. (b) The contact angle is calculated as the angle of a tangent at the point of intersection of the circle and the substrate. To get the contact angle of the water droplet the provided value needs to be subtracted from 180 degrees.

2.6 Sample preparation protein binding

To unveil the protein binding properties of the polymer structures a fluorophore protein conjugate was incubated on the samples. Bovine from serum albumin was used as protein as BSA is low cost, available with a wide range of conjugated fluorophores and the binding properties of BSA are well known. BSA is often used as a passivation or blocking agent on all kinds of substrate as the binding of BSA is highly nonspecific. [40] During XFEL experiments proteins are present over a long period of time. To mimic the binding of proteins within the microfluidic device the BSA is used at low concentration and is only incubated for a short period of time due to its fast binding rate. To observe the binding of low concentration of protein fluorophore conjugates a fluorophore with high photon yield (number of photons detectable after excitement) is required. Alexa Fluor 488 is known to be a bright and stable fluorophore. [41]
The BSA Alexa Fluor 488 was prepared as a 0,1mg/mL solution in phosphate buffered saline (PBS) and incubated on the samples for 5 minutes at room temperature. After incubation, the samples were washed 5 times with PBS to remove any unbound proteins and reduce the background signal.

2.7 Fluorescence Imaging

Fluorescence imaging is a powerful tool which is used in a broad field of research. The resolution is higher compared to standard white light microscopy and via labelling target molecules specifically with fluorophores various processes can be observed. Fluorescence microscopy is mainly used to study living cells and tissue as this technique allows for protein tracing to visualize processes within living specimen. [42] Fluorophores are molecules which are pumped into an excited state by absorption of photons of a certain wavelength. In the process of relaxation, the excess energy is emitted as photons which can be detected and processed into an image. A simple Jablonski diagram depicting the energy levels of a fluorophore and explaining this process is displayed in Figure 10a. [43] The difference in the excitation maximum and the emission maximum (shift from excited state S_2 down to S_1) the so called Stokes Shift allows to image the sample using the same objective for excitation and emission. [44] A dichroic mirror is an optical element, which is reflective for a certain wavelength and transmits light at a slightly different wavelength. As some energy is lost as atomic vibrations in the fluorophores and as heat the emitted photon is of different energy resulting in a different wavelength. In a fluorescence microscope the illumination source is either a laser or a mercury lamp. The excitation illumination is guided towards the specimen through a set of mirrors and filters. The emitted photons are collected by the same objective and guided towards the detector via a dichroic mirror (Figure 10b). The ocular to observe specimen in white light microscopy is usually replaced by an EMCCD camera. A photomultiplier is used to enhance the signal and improve the image.

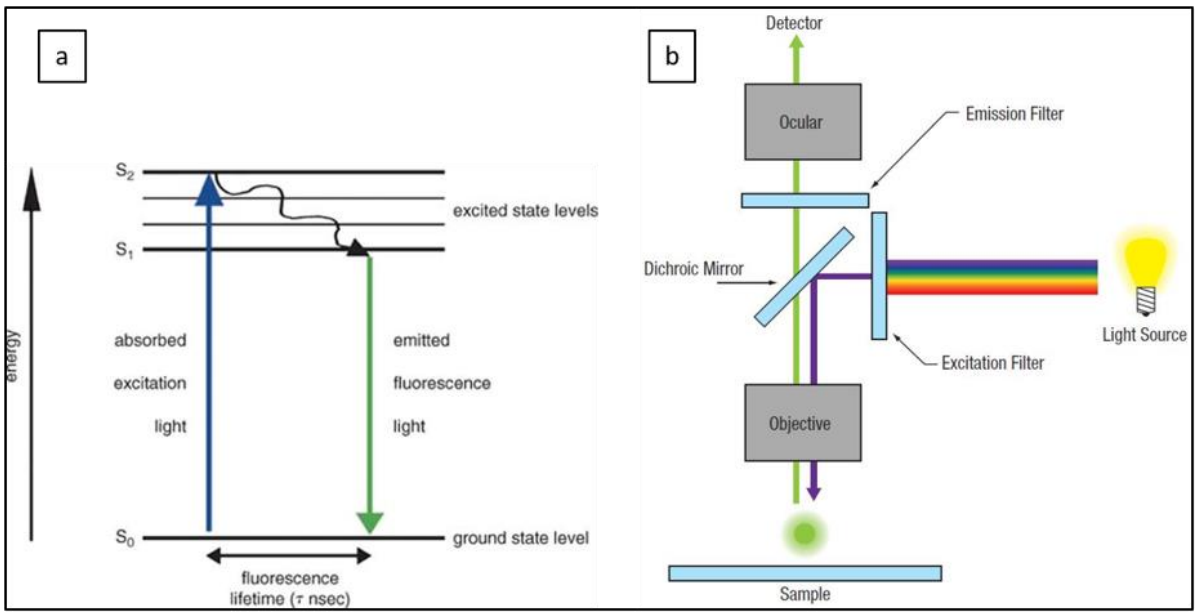

Figure 10 (a) Jablonski diagram showing the different energy levels of a fluorophore. Upon excitement at a certain wavelength the fluorophore gets pushed into the excited state. After a short period of time the fluorophore relaxes and releases the energy difference as photons. The Jablonski diagram provides information about the different energy levels and the time between excitement and relaxation. [43] (b) Standard setup for a fluorescence microscope. A sample is excited via a proper light source (e.g. laser) The light is guided by a dichroic mirror towards the specimen. As the fluorophores radiate at a different wavelength due to the Stokes shift the light is transmitted at the dichroic mirror. An emission filter is used to further enhance the signal. [45]

The excitation wavelength is chosen either by the used laser or by inserting an excitation laser into the illumination pathway. The used fluorophore Alexa Fluor 488 shows an excitation maximum around 490 nm and an emission maximum around 525 nm. Therefore, an excitation filter 470/20 nm and an emission filter 525/25 nm were chosen. The sample was illuminated by a mercury lamp and the images were taken with an illumination time of 10ms. All images were acquired at 20x magnification using an inverted Olympus iX71.
The images were processed in ImageJ. The signal along the PETA and PEGDA structures have been measured on several lines and the mean value was taken for further analysis. The background signal was calculated as mean value across multiple areas without polymer lines. The difference between the polymer lines and the background was calculated by using the mean values of the signals. The calculation of bound proteins on the different polymers and the substrate was not conducted during this work.

3 Results

Here, I present the results for the presented initial problem using the techniques described above. All experiments were conducted in the laboratory of Dr. Alexandra Ros at the Biodesign Center at Arizona State University.

3.1 2D and 3D modeling

For the hydrophobic surface coating and the protein binding properties of acrylate structures several designs were required. Figure 11 shows the designs of the 5x5mm block in (a) to test the crosslinking of

the DFHA on top of a PETA surface, the 2D grid in (b) for comparison of protein binding properties of PETA and PEGDA, a test channel with one and a test channel with 3 channels in (c, d) with a radius of25 µm to apply both approaches in a 3D device. Block designs for PETA and PEGDA structures on the same sample and other designs for 3D channels have been discarded as the first results of experiments were not promising.

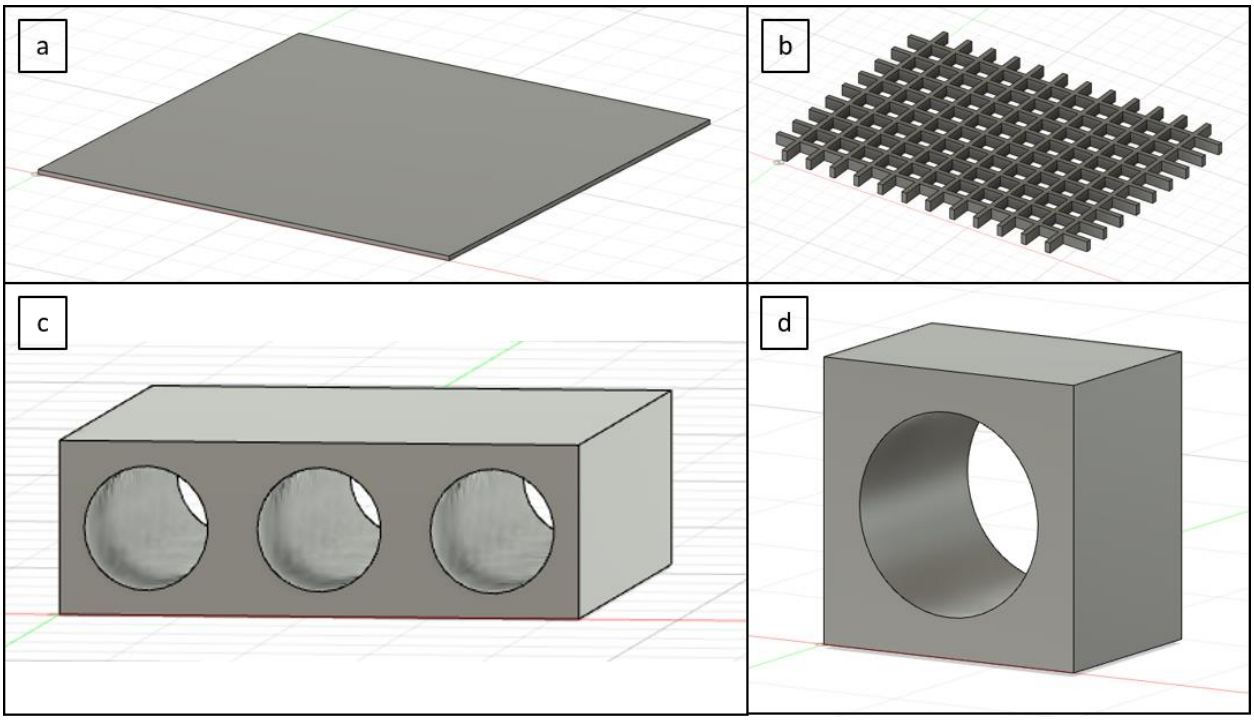

Figure 11 Designs constructed using Fusion360: (a) 5x5mm with a height of 50 µm structure to print a test PETA surface for a hydrophobic coating. (b) test grid of PETA and PEGDA lines to test the protein binding properties of the two different photoresists. (c, d) 3D channels with a radius of 25 µm to test the hydrophobic coating inside a 3D device and analyze the protein binding within a channel.

In the code for the 3D printing system the laser power, the writing speed have been adjusted depending on the photoresist. When decreasing the writing speed while increasing the laser power micro explosions occur during the printing leading to air bubbles within the structures. Air bubbles in the structure are especially crucial in fluorescence imaging as the excitation illumination gets refracted at the air polymer interface which results in a high background signal. Since Nanoscribe does not provide the user with the actual data for the used laser power and the setup does not allow to measure the laser power at the objective, the best approach was to increase the writing speed to the maximum of 10cm/s for noncrucial parts and reduce the laser power to a value at which no micro explosions occur. Furthermore, the system requires a stage correction if the system is not operated with the standard photoresist provided by the company. This stage correction accounts for the mismatch in refractive index between the ITO glass slide and PETA/PEGDA and the resulting aberration. Describe automatically generates a code file describing the path of the laser and setting the laser power and writing speed along the path. The resulting code after the implementation of the optimization for the photoresist and the stage correction can be seen in Figure 12.

PEGDA_lines_V2_job.gwl | channel_capillary_v2_PEGDA_job.gwl | **channel_capillary_v2_job.gwl** | channel_capillary_V1_job.gwl

```
% File generated by DeScribe 2.5.1

% System initialization
InvertZAxis 1

% Writing configuration
GalvoScanMode
ContinuousMode
PiezoSettlingTime 20
GalvoAcceleration 5
StageVelocity 200

% Scan field offsets
XOffset 0
YOffset 0
ZOffset 0

%% StageCorrection %%

var $SCSx = 1.0015
var $SCSy = 1.0015
var $SCAx = 0.26
var $SCAy = 0.18
StageCorrectionOn
StageCorrectionStretchX $SCSx
StageCorrectionStretchY $SCSy
StageCorrectionAngleX $SCAx
StageCorrectionAngleY $SCAy

% Writing parameters
PowerScaling 1.0

% Contour writing parameters
var $contourLaserPower = 85
var $contourScanSpeed = 100000

% Solid hatch lines writing parameters
var $solidLaserPower = 100
var $solidScanSpeed = 80000

% Base writing parameters
var $baseLaserPower = $contourLaserPower
var $baseScanSpeed = $contourScanSpeed

var $interfacePos = 0.5

% Include slicer output
include channel_capillary_v2_data.gwl
```

Figure 12 Generated code using Describe to translate the designed structure into a workflow for the 3D printer. The laser power and the writing speed require adjustments according to the used photoresist. The stage correction is needed to compensate the refractive index mismatch between the ITO glass slide and the photoresist PETA/PEGDA. This code allows to print any desired 2D or 3D pattern. The laser follows a path described within the code setting the laser power and writing speed accordingly.

3.2 Contact angle measurement

To verify the effect of a surface coating on acrylate structures PETA and PEGDA surfaces have been fabricated by spin coating the photoresist on a substrate, UV-curing and developing the polymer and measuring the contact angle. As a result, the contact angle on PETA has been measured at 60 degrees (Figure 13a) and for PEGDA at 60 degrees (Figure 13b)

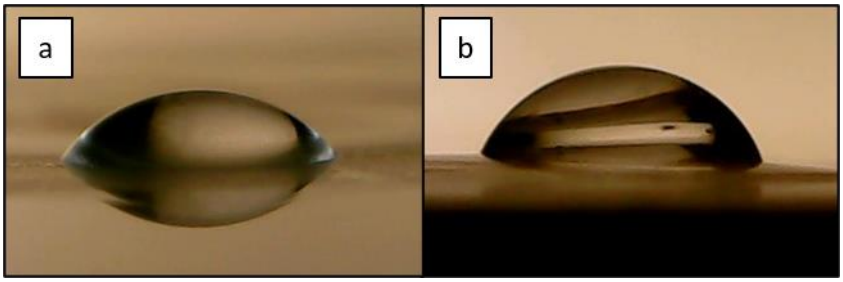

Figure 13 Water droplet on a fabricated PETA (a) and PEGDA (b) surfaces yielding contact angles of 60 degrees for PETA and 60 degrees for PEGDA.

3.3 Hydrophobic surface coating

To obtain a hydrophobic surface coating on acrylate structures the previously described fluorinated acrylate DFHA was chosen. To get an insight on the effects of the addition of DFHA to a polymer several ratios of PETA and DFHA have been tested. As previously described Irgacure 819 offers good properties regarding polymerization and low autofluorescence and therefore, this photoinitiator was chosen and added at 1wt% to all mixtures.
In first trials the mixtures of the monomers have been spin coated on glass slides and illuminated with UV light at 365nm for up to 2 minutes. The spin coating process required optimizations as the viscosity decreases by a margin as the amount off DFHA increases. Therefore, the spin speed, the acceleration and the time has been adjusted accordingly to Table 1. The acceleration setting is a fixed value when using a Laurell WS-650-8B as spin coating device. Trials of printing the mixtures with the Nanoscribe setup have not been successful as the photoresist requires high energy for polymerization. The only way to polymerize the photoresist was to reduce the writing speed by a margin leading to a significant increase in the required time to fabricate an area big enough to measure the contact angle of a water droplet on top.

Table 1 Spin coating settings for hydrophobic polymers on test surface using a Laurell WS-650-8B

Photoresist	Spin speed	Acceleration	time
PETA	2500 rpm	5	15 seconds
PEGDA	2000 rpm	5	10 seconds
4: 1 PETA - DFHA	2500 rpm	5	15 seconds
2:1 PETA - DFHA	2000 rpm	5	10 seconds
1: 1 PETA - DFHA	1000 rpm	5	10 seconds
2:1 DFHA – PETA	1000 rpm	3	7 seconds

As a first result it has been observed that the photoresist acts differently with increasing proportion of DFHA. Besides the required adjustments for the spin coating due to the viscosity change the polymerization rate decreased as well. As described previously, PETA shows fast polymerization but with increasing proportion of DFHA the illumination time had to be increased. For the various photoresists, illumination protocols according to Table 2 have been established.

Table 2 Illumination protocol for hydrophobic polymers on a test surface at 365 nm

Photoresist	Illumination time

PETA	10 seconds
PEGDA	10 seconds
4: 1 PETA - DFHA	10 seconds
2:1 PETA - DFHA	30 seconds
1: 1 PETA - DFHA	1 minute
2:1 DFHA – PETA	2 minutes

After refining the procedure for obtaining acrylate surfaces the contact angle was measured to unveil the increase in hydrophobicity. For each surface multiple measurements have been done to obtain statistical relevant data. For comparison, a boxplot has been produced. As Table 3 and Figure 14 show the effect of the addition of DFHA to PETA did not have the desired effect on the hydrophobic behavior of the surface. The photoresist containing DFHA at a ratio of 2:1 to PETA showed a maximum of 70 degrees (circle fit). The increase of 10 degrees is not considered high enough to show a shift towards hydrophobic properties of the acrylate surface through addition of a fluorinated acrylate. The acquired data is shown as a boxplot in Figure 15 representing all measurements across the samples. This result leads to the assumption that the fluorine groups tend to not be present in a high enough number on the surface to increase the hydrophobicity of the polymer as observed in the application of other fluorinated surface coatings.

Table 3 Resulting contact angle for circle and elliptical fitting using the ImageJ toolbox on multiple samples

Photoresist	Contact angle circle fit	Contact angle elliptical fit
PETA	59,94° ± 4,89°	63,68° ± 4,06°
PEGDA	59,71° ± 4,02°	64,14° ± 5,63°
PETA 4:1 DFHA	63,08° ± 1,03°	64,70° ± 1,64°
PETA 2:1 DFHA	64,25° ± 1,67°	65,87° ± 4,12°
PETA 1:1 DFHA	68,17° ± 2,34°	70,85° ± 2,92°
DFHA 2:1 PETA	69,25° ± 2,73°	71,67° ± 4,07°

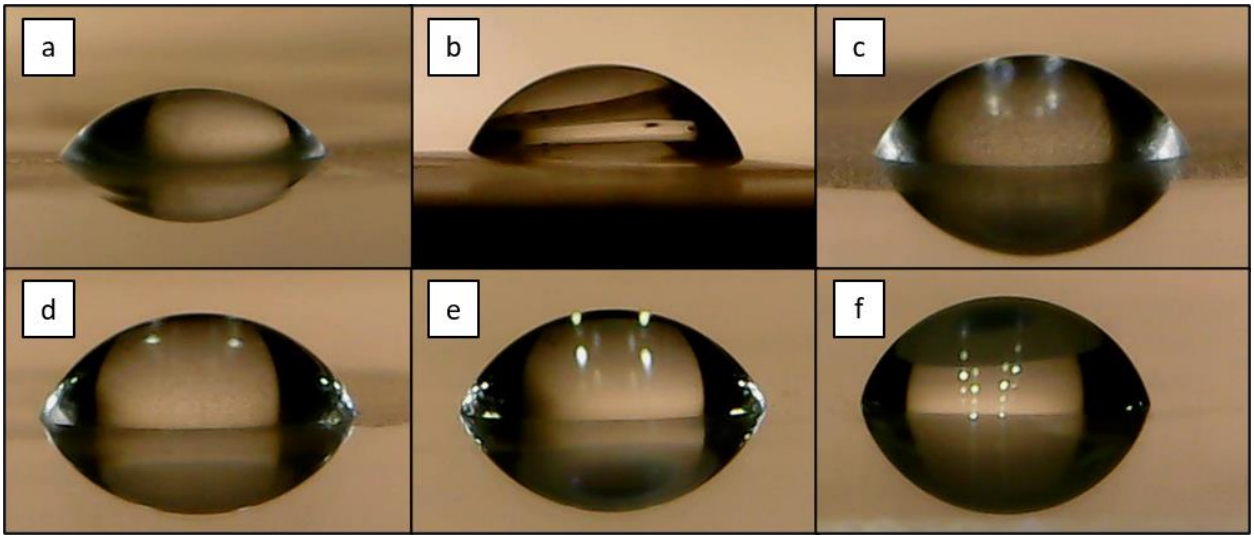

Figure 14 Water droplets on various spin coated photoresist surfaces for contact angle measurements. (a) PETA, (b) PEGDA, (c) PETA 4:1 DFHA, (d) PETA 2:1 DFHA, (e) PETA 1:1 DFHA, (f) DFHA 2:1 PETA: The contact angle difference between pure PETA and the mixture with the highest amount of DFHA shows a difference in contact angle of 10

degrees. To consider the change of the surface towards a hydrophobic behavior the increase of 10 degrees to a maximum of 70 degrees in the circle fit for the photoresist DFHA 2:1 PETA is not high enough.

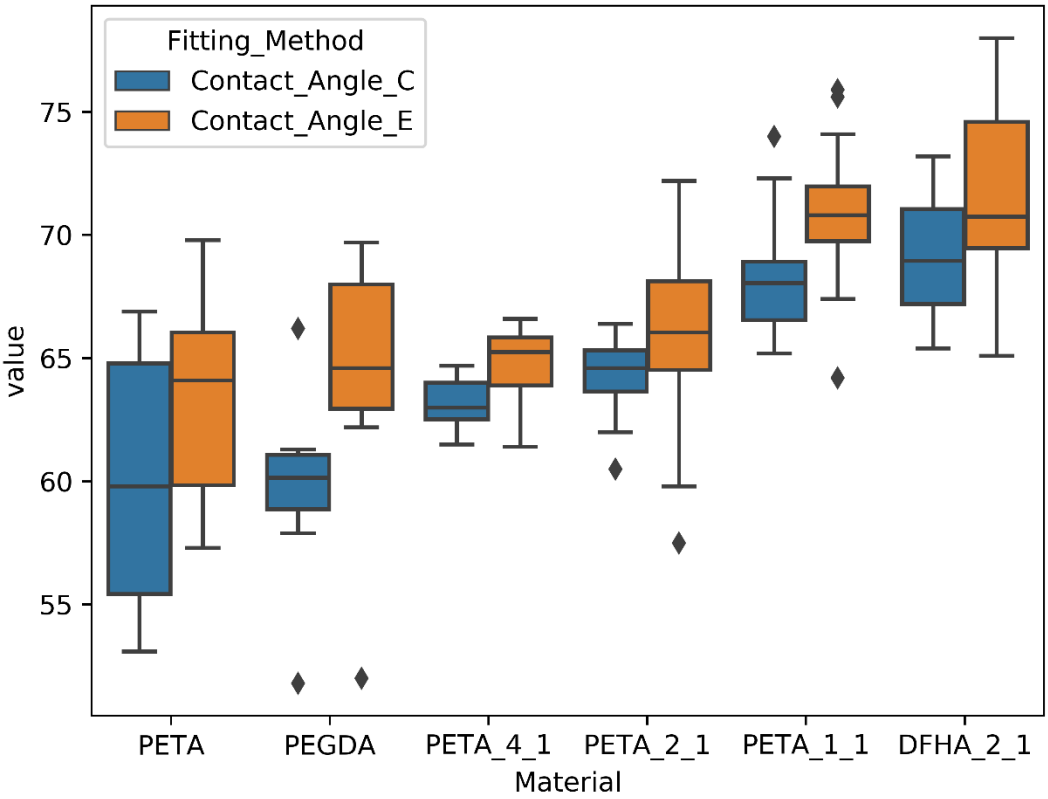

Figure 15 Display of the data acquired for the contact angle measurements across multiple samples and measurements as boxplot. The data indicates an insufficient increase in the contact angle to strengthen the assumption of one of the photoresists being suitable for a hydrophobic surface coating.

Further testing of hydrophobic surface coatings was done on printed PETA structures and spin coated PEGDA surfaces. The PETA structures were fabricated using the Nanoscribe system. The writing parameters of writing speed and laser power were optimized to the maximum of 10cm/s at 100% laser power.

Directly crosslinking the pure DFHA to either PETA or PEGDA structures could not be achieved using the Nanoscribe system as the system requires to use autofocusing to find the surface via impedance measurement. The already printed structures hindered the system from using the Auto-Focus function and therefore a different approach was required. Furthermore, the low viscosity of the fluorinated acrylate hindered the application of DiLL as a droplet of photoresist would drop into the system instead of staying on the substrate to be processed.

As a solution the UV-lamp used to polymerize the spin coated surfaces was used to directly crosslink the DFHA to the acrylate structures. Therefore, 1wt% of Irgacure 819 was dissolved in DFHA using a high performance ultrasonication bath and applied to the structure. The surface was illuminated for 30 minutes at 365 nm. After developing the structure in Acetone and rinsing it with Isopropanol the contact angle was measured. As seen in Figure 16 PETA and PEGDA structures were coated with DFHA yielding an

increase in contact angle summarized in Table 4. The increase of the contact angle of 42 degrees on the PETA structure and 40 degrees on the PEGDA structure to a maximum of 102 degrees shown as boxplot in Figure 17 indicate the introduction of a hydrophobic surface coating.
The required time to crosslink a layer of fluorinate acrylate on top of a PETA or PEGDA surface strengthens the assumption that the polymerization of the DFHA in the photoresist used during the spin coating experiments shows significantly slower polymerization rates and thus being present in a much lower quantity at the surface of the cured polymer.

Table 4 Resulting contact angle after coating the surface of PETA and PEGDA structures with DFHA

Photoresist	Contact angle circle fit	Contact angle elliptical fit
PETA	59,94° ± 4,89°	63,68° ± 4,06°
PEGDA	59,71° ± 4,02°	64,14° ± 5,63°
PETA coated with DFHA	101,72° ± 4,94°	103,32° ± 5,21°
PEGDA coated with DFHA	100,50° ± 4,10°	100,63° ± 3,88°

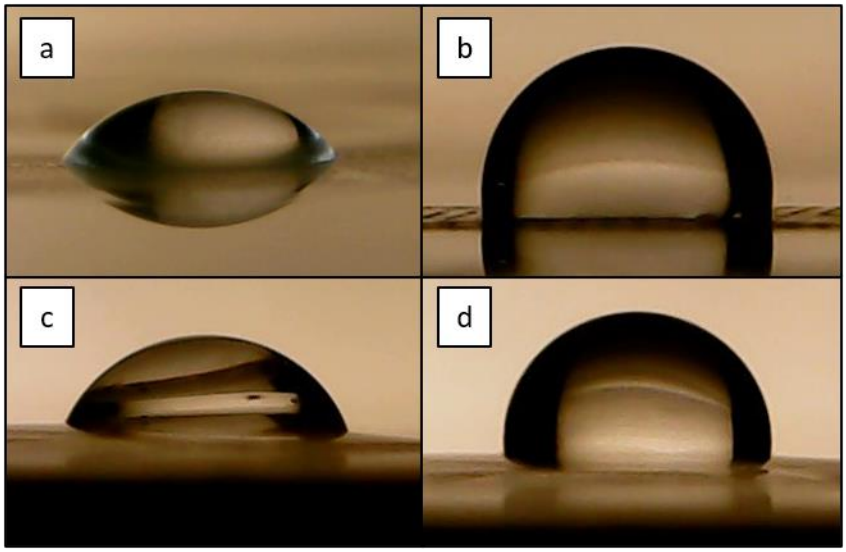

Figure 16 Water droplets on various acrylate surfaces. (a) PETA, (b) PETA coated with DFHA, (c) PEGDA, (d) PEGDA coated with DFHA. The coating procedure with DFHA using a UV lamp for crosslinking yielded an increase in contact angle of 42 degrees on the PETA surface and of 40 degrees on the PEGDA surface. The resulting contact angles of above 100 degrees show the introduction of a hydrophobic surface coating via crosslinking of two acrylates.

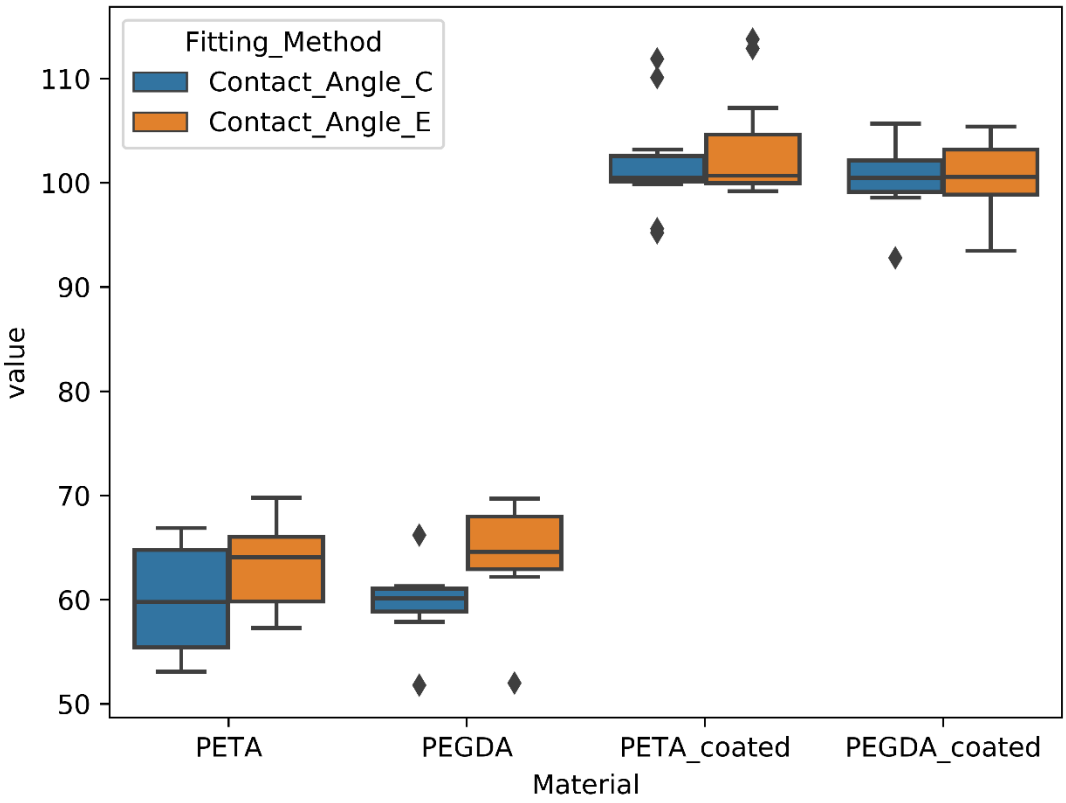

Figure 17 Boxplot of the data acquired for all measurements on coated and uncoated PETA and PEGDA surfaces. The difference in the contact angle strengthens the assumption of the introduction of a hydrophobic surface. Further statistical test will allow to test if the difference is significant for both acrylates.

The findings acquired during the 2D experiments were converted to a 3D approach. The DFHA was applied to a 3D channel. Before the coating procedure the interaction of water within the channels was observed and imaged. After testing the hydrophobicity inside the channel DFHA was coated by illuminating the filled channel for 30min at 365 nm. The coating was developed by submerging the structure into Acetone for 5 minutes and 2 minutes in Isopropanol. The channels were dried to avoid interactions of water with residuals of Acetone or Isopropanol. To test the effect of coating water was applied to channels in the same way it has been applied to the uncoated structure. The coating hindered the interactions between the channel and a droplet of water observed before the procedure entirely. Figure 18 Depicts the interactions of water and the PETA channel before and after the coating procedure. It can be seen clearly that all channels are filled with water (Figure 18a) as the capillary forces suck water inside the channels. A meniscus of water is formed as the water evaporates inside the channel and migrates through the channel (Figure 18b). After the coating procedure the water droplet does not interact with the channels at all (Figure 18c).

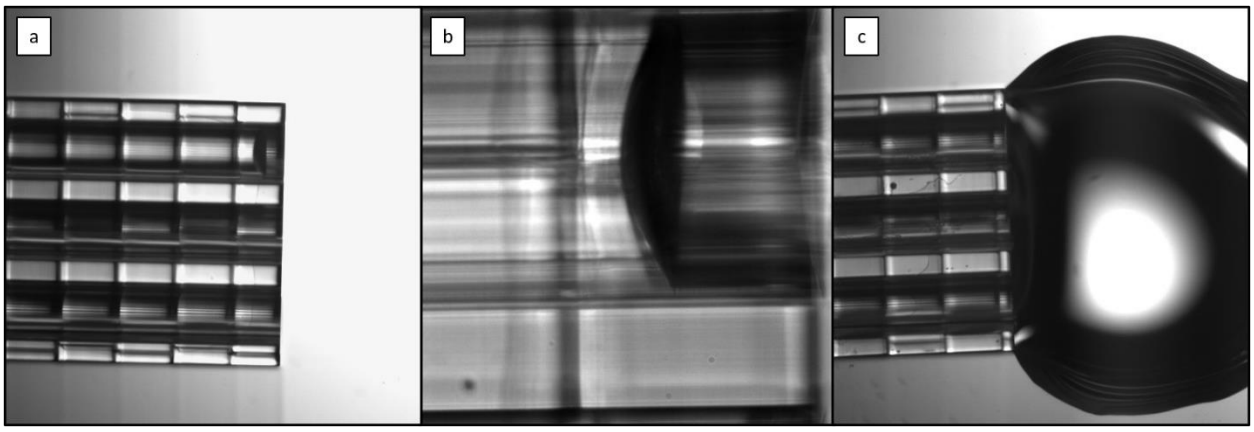

Figure 18 3D Interactions of water and a PETA channel before and after coating procedure with DFHA. (a) Interaction of water and the channels. The channels get filled immediately due to capillary forces sucking water inside the channels. (b) A water meniscus is formed as the water starts to evaporate and the remaining water migrates through the channel. (c) After the DFHA coating procedure no interaction between the channel and water is observable. The introduced hydrophobicity hinders the capillary forces from sucking water into the channels.

3.4 Protein binding properties

A photoresist consisting of PEGDA and PETA at a ratio of 4:1 was optimized regarding writing speed and laser power to fabricate 2D lines for a grid of alternating photoresist lines and a 3D channel. Writing speeds of 8.5cm/s for the contour part of the structure at 90% laser power and 10cm/s at 100% laser power have been found to yield the best results. Lowering the laser power resulted in collapsing structures while the decrease in writing speed to compensate for the reduction of absorbed photons led to micro explosions. For the PETA lines the same settings have been used as for the structures fabricated during the hydrophobicity experiments.

First tries to write PETA and PEGDA structures on the same sample brought up the same problems which occured during the attempts to coat the fluorinated acrylate directly using the Nanoscribe system. Either the system was not able to find the surface at all because of the impedance mismatch, or the system was able to start a writing process but the structures were not aligned properly afterwards and a comparison of the photoresists was not possible. A switch in the model from alternating blocks (PETA – PEGDA – PETA) (Figure 19a) towards the presented model of the grid of horizontal lines of PEGDA and vertical lines of PETA in chapter 3.1 allowed to print both photoresist on the same sample (Figure 19b).

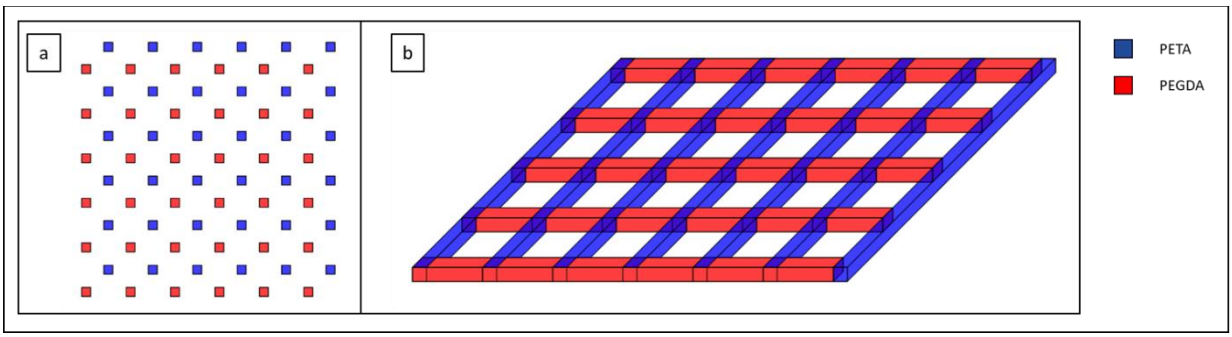

Figure 19 Fabrication approaches for PETA and PEGDA 2D structures on one sample. (a) Alternating blocks have been the first approach to print both photoresist side by side. Problems with the Auto-Focus function and the alignment of the structures required a change in the design. (b) A switch towards a grid of alternating lines solved both problems.

White light (Figure 20a ,b) and fluorescence images (Figure 20c,d) of the block and the grid designs show that the grid provided enough area of photoresist to measure the difference in signal. Furthermore, the grid was more stable during the incubation and the measurements as the structures did not float away in contrast to the blocks where most of the structures started floating during the incubation or were lost during the development. Blue borders indicate PETA and red borders indicate PEGDA.

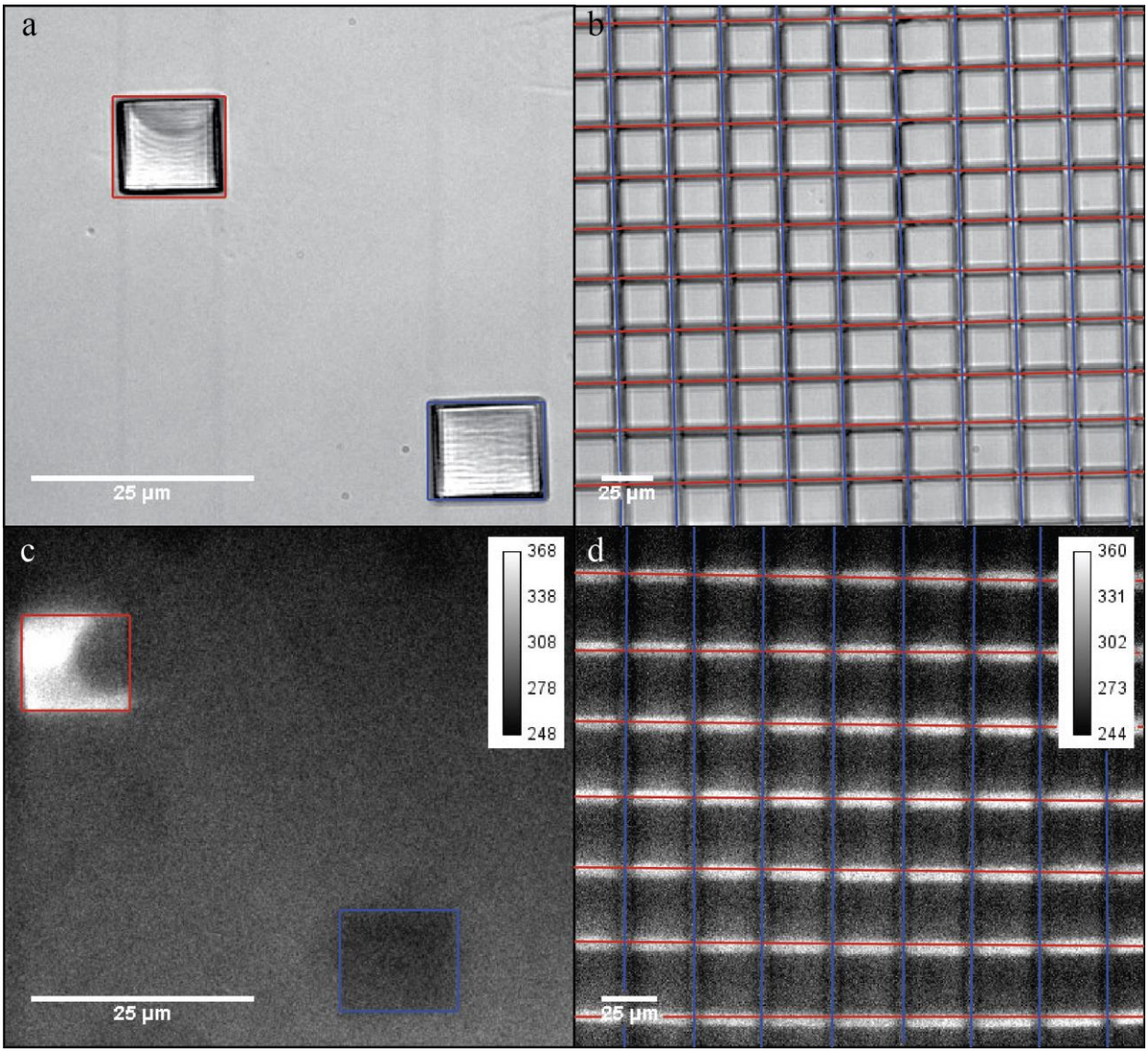

Figure 20 White light and fluorescence images of the 2D structures to test the protein binding properties of acrylate structures. (a) Block design of PETA and PEGDA side by side. During the development and the incubation with the protein solution most of the structures started floating and were lost. (b) Grid design of vertical PETA lines and horizontal PEGDA lines. (c, d) Fluorescence images of the designs showing the lack of area to measure the difference in fluorescence signal across multiple measurements on one sample for the block design.

After the incubation of the structure with the BSA Alexa Fluor 488 conjugate the fluorescence images were analyzed to see the difference in fluorescence signal on the PEGDA lines, the PETA lines and the background signal on the ITO glass slide. The difference in fluorescence signal represents the difference

in nonspecific protein binding of the BSA on the different photoresists and the substrate. As a result, the signal on the PEGDA lines is 30% lower compared to the PETA lines (Figure 21).

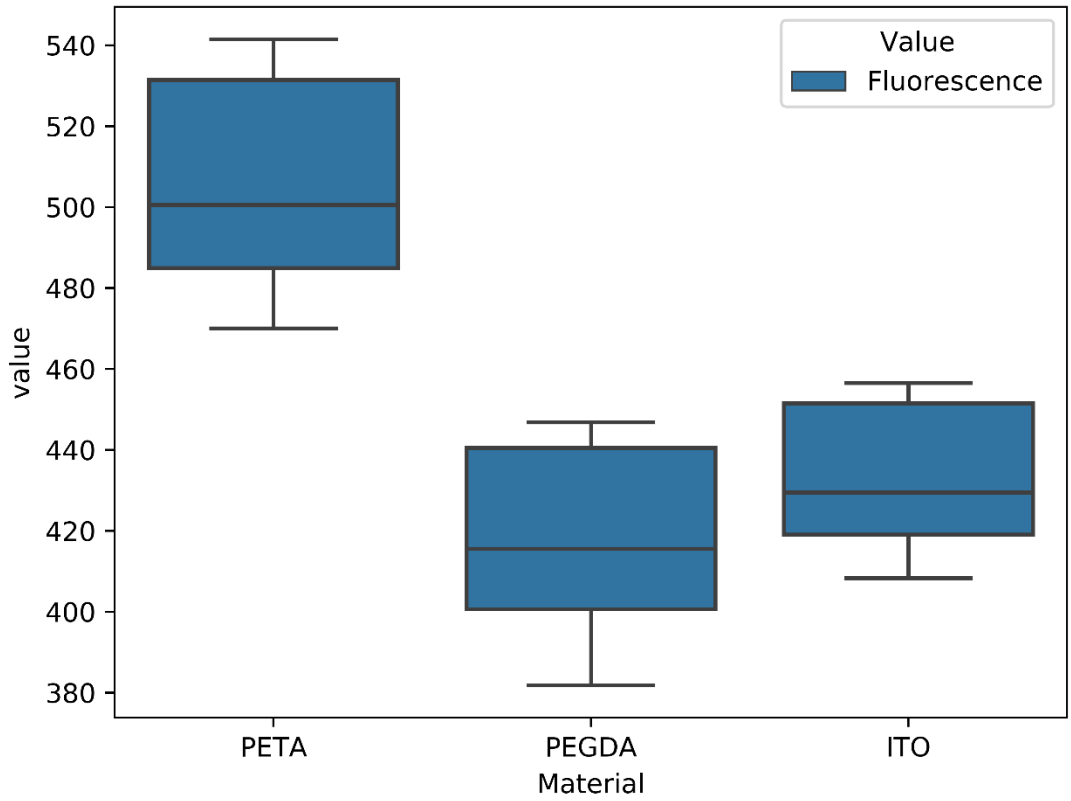

Figure 21 A boxplot has been used to compare the evaluated signals across multiple samples. The signal on PETA is 30% higher than on the PEGDA lines. The difference between PEGDA and the ITO glass slide is around 5%.

The signal of the photoresists and the background were analyzed on multiple areas on one sample and the difference between the signals was also compared across different samples (Table 5).

Table 5 Measured intensity across multiple areas of photoresist and background 2D grid

Photoresist	Intensity
PETA	506,63 ± 26,14 counts
PEGDA	419,00 ± 23,80 counts
Background (ITO-glass slide)	433,96 ± 17,42 counts

In the 3D approach the same problem of the required autofocusing hindered the combination of a PEGDA and PETA channel side by side. As the 3D channel is much higher than the lines previously used in the 2D printing the printer destroyed the structures already written in the first printing procedure. To test if a similar result could still be achieved in a 3D channel PEGDA and PETA channels were fabricated on separate ITO glass slides.

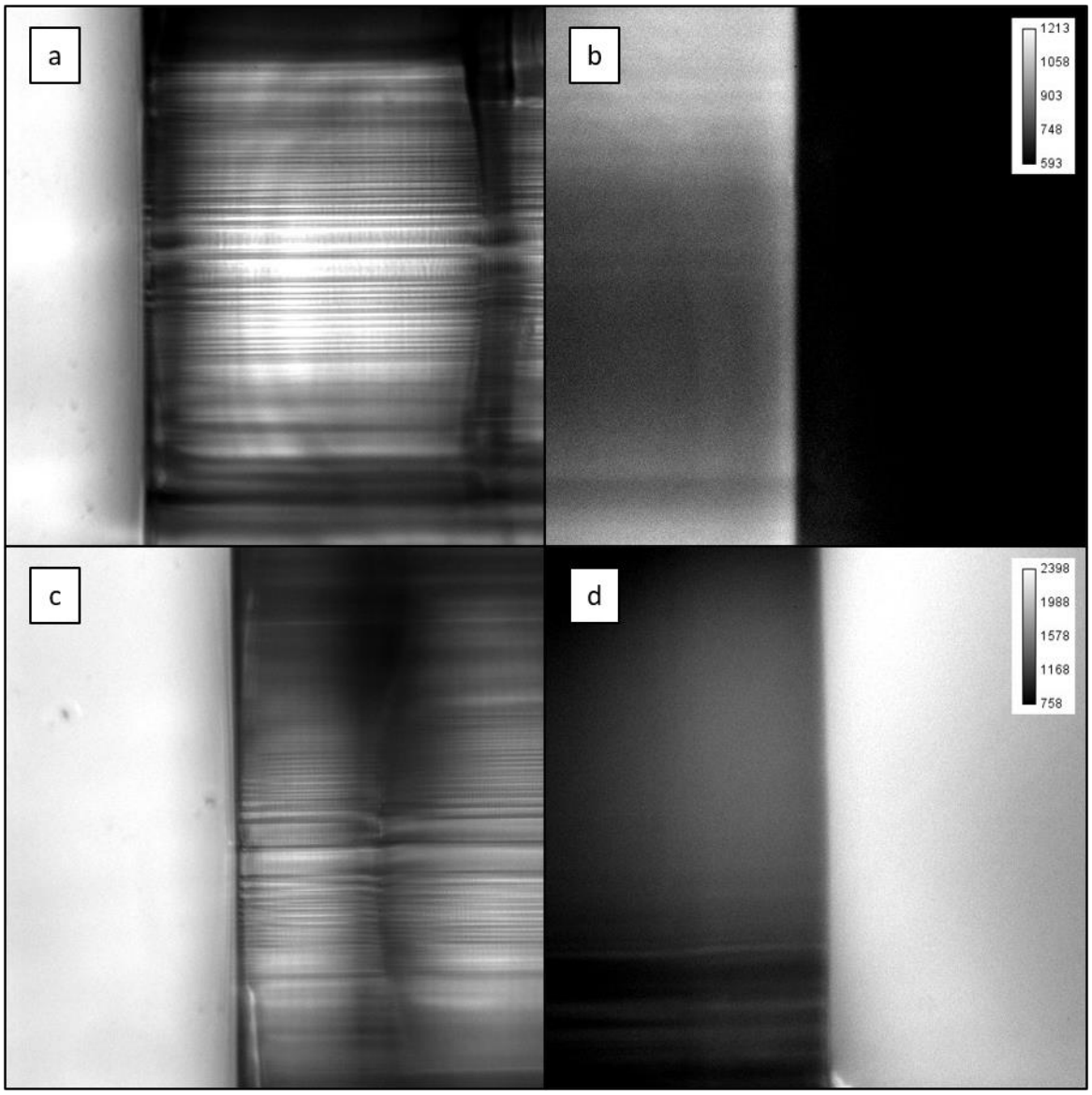

Figure 22 White light and fluorescence images of 3D channels. (a) White light image of the PETA channel. (b) Fluorescence image of the PETA channel indicating a much higher signal of bound BSA to the PETA structure. (c) White light image of the PEGDA channel. (d) Fluorescence image of the PEGDA channel showing a promising difference between signal of the ITO glass slide and the polymer structure.

Despite the test channel being several micrometers above the ITO surface the background signal generated by the bound BSA on the substrate is still high in comparison to the signals inside the channel. Fortunately, the background signal of the ITO glass slides has been found to be similar across the samples making a comparison of the different samples possible (fluctuations around 5-7%). The 3D experiments showed a big difference in the intensity of the fluorescence signal between PETA and PEGDA. Bound BSA on the PETA structures emitted signals up to 90% higher than the signal on PEGDA structures (Figure 23). The difference between the signal within the PEGDA channel and the bound proteins on the IOT glass slide are more obvious than in the 2D experiments.

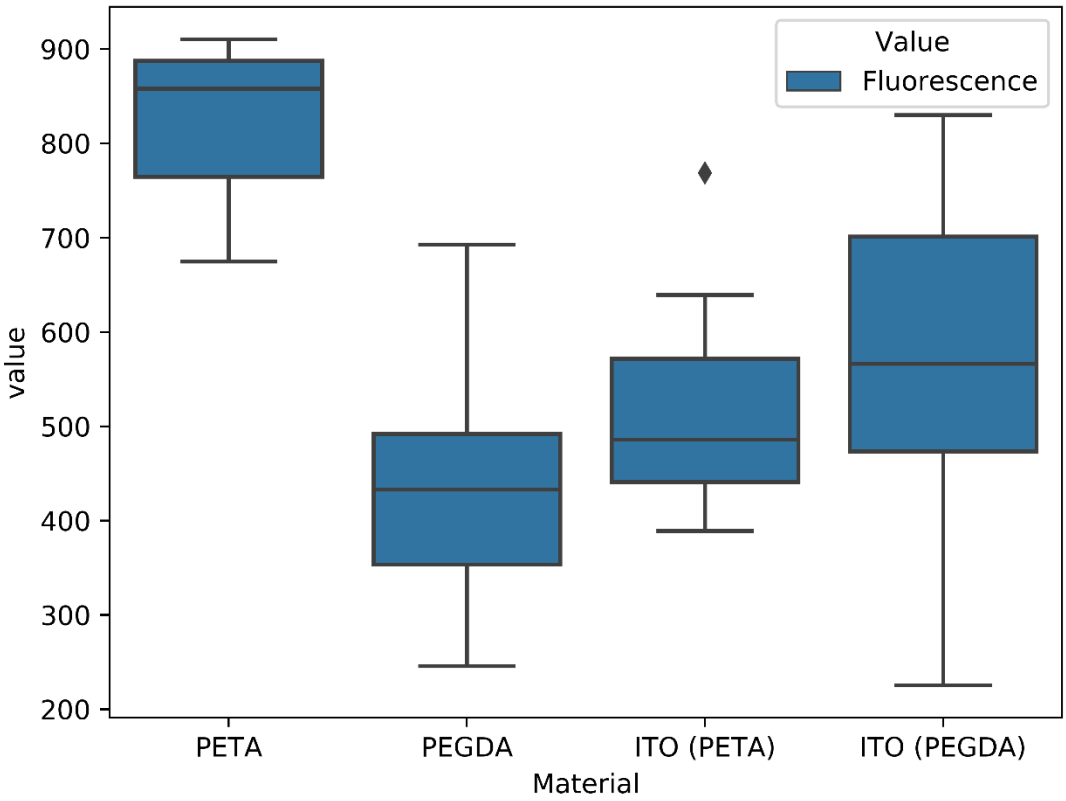

Figure 23 The comparison of the signals with a boxplot showed a obvious difference in the signal between the used photoresist. The bound proteins on PETA emitted signals up to 90% higher than on the PEGDA structure. The big difference in standard deviation in comparison to the 2D experiments may arise from the difficulties of washing away unbound proteins from within the 3D channel. Despite the background signal due to the remaining proteins within the channel the difference of the protein binding properties of PETA and PEGDA can be seen.

The 3D experiments have been conducted 5 times for each photoresist. The high standard deviation compared to the evaluation of the 2D experiments may arise due to the unbound proteins within the channel. Flushing the channel to wash away the excess proteins has been tricky in order not to destroy the channel.

Table 6 Measured intensity across multiple areas of photoresist and background 3D channel

Photoresist	Intensity
PETA	829,91 ± 83,15 counts
PEGDA	433,28 ± 134,45 counts
Background (ITO-glass slide) PETA	524,30 ± 133,77 counts
Background (ITO-glass slide) PEGDA	559,30 ± 195,87 counts

4 Conclusion and Outlook

The main parts of the initial situation and the problems encounter on the path towards the solution have been solved. A coating procedure for 2D and 3D acrylate structures using an optical setup was developed and a protocol to use various acrylates with the 3D printer Nanoscribe Photonic Professional GT was established. The reduction of nonspecific protein binding was achieved by adding PEGDA to the primary monomer PETA.

Further research on the hydrophobic surface coating will include partial coating of a 3D channel. A promising approach to achieve hydrophobic and hydrophilic surface areas within one 3D microfluidic device is to illuminate only one part of the device using a photomask resulting in crosslinking of the DFHA only in illuminated parts. This will allow variable flow conditions within one microfluidic device. Variable flow conditions will be of importance for ongoing research on the synchronization of protein droplet delivery and the pulse train at XFEL facilities.

To decrease the background signal in the 3D channel and solve the problem of detaching of the structure during the incubation with the protein solution a new test channel has been designed with the possibility to attach capillaries to channel. In this case no protein will bind on the substrate and the acquired signal will only result from nonspecifically bound BSA within the channel. As the channel design has been switched towards a rectangular shape focusing on the interface of the bound protein will be easier and the resulting images will be easier to compare (Figure 24). The incubation and flushing the channel afterwards to remove any unbound proteins is also enhance using this design. As the problem of detaching of the structure will be solve as well, long term binding studies within the channel under flow conditions are possible. This approach will allow to test the introduced protocol in an experiment mimicking the flow conditions used in crystallography microfluidic devices. The measured “counts” for the signals can be used to calculate the detected photons. As the photon yield of Alexa 488 is known the amount of bound proteins to the structures can be calculated. This calculation would allow to design an experiment to test the protein binding on PETA and PEGDA structures over time.

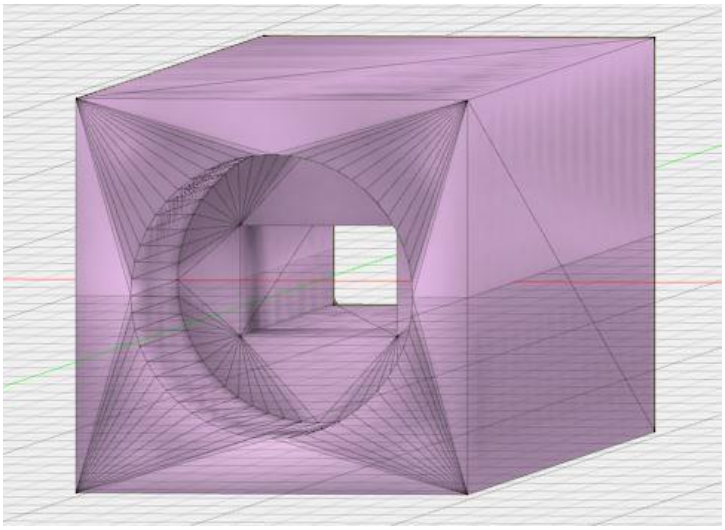

Figure 24 New design for a 3D channel. Inlet and outlet designed to allow the attachment of capillaries. The rectangular shaped channel allows to focus easier on the surface after the incubation with proteins. The fluorescence signal will result solely from nonspecific bound proteins within the channel. Applying the protein solution through a capillary allows easier flushing of capillary washing away unbound proteins and lowering the background signal.

To verify the effect of PEGDA as a modifying agent to PETA to reduce nonspecific protein binding further image processing is required. Background correction and subtraction will be used to normalize the signals across multiple images. This method will allow to compare the samples and images and analyze the data more precisely. Further analysis will allow to prove a significance in signal difference between pure PETA and the PEGDA modified structures.
Statistical test will prove that the increase in contact angle after the coating procedure provided significant data.

All results presented in this report have been accomplished during my research stay at Arizona State University. Further processing and analysis of the fluorescence images and the data acquire by the contact angle measurements will be part of my Master thesis which will be finished in June 2020. The design and protocols for further testing of the coating using the photomask and the new design for the channel with attached capillaries have been developed but could not be tested by the end of my research stay.

I want to thank the Austrian Marshall Plan Foundation for their support. Without the support of this foundation this interesting research project would have not been possible.

List of Tables

List of Figures

References

[1] M. Maeki, H. Yamaguchi, M. Tokeshi, and M. Miyazaki, “Microfluidic Approaches for Protein Crystal Structure Analysis,” *Anal. Sci. Int. J. Jpn. Soc. Anal. Chem.*, vol. 32, no. 1, pp. 3–9, 2016, doi: 10.2116/analsci.32.3.

[2] “X-ray Free Electron Lasers - A Revolution in Structural Biology | Sebastien Boutet | Springer,” Nov. 27, 2019. https://www.springer.com/gp/book/9783030005504 (accessed Nov. 27, 2019).

[3] “Serial femtosecond crystallography: A revolution in structural biology. - PubMed - NCBI,” Nov. 27, 2019. https://www.ncbi.nlm.nih.gov/pubmed/27143509 (accessed Nov. 27, 2019).

[4] R. B. Doak *et al.*, “Microscopic linear liquid streams in vacuum: Injection of solvated biological samples into X-ray free electron lasers,” *AIP Conf. Proc.*, vol. 1501, no. 1, pp. 1314–1323, Nov. 2012, doi: 10.1063/1.4769693.

[5] C. Gisriel *et al.*, “Membrane protein megahertz crystallography at the European XFEL,” *Nat. Commun.*, vol. 10, no. 1, pp. 1–11, Nov. 2019, doi: 10.1038/s41467-019-12955-3.

[6] J. Blümmel *et al.*, “Protein repellent properties of covalently attached PEG coatings on nanostructured SiO(2)-based interfaces,” *Biomaterials*, vol. 28, no. 32, pp. 4739–4747, Nov. 2007, doi: 10.1016/j.biomaterials.2007.07.038.

[7] A. Echelmeier *et al.*, “3D printed droplet generation devices for serial femtosecond crystallography enabled by surface coating,” *J. Appl. Crystallogr.*, vol. 52, no. Pt 5, pp. 997–1008, Oct. 2019, doi: 10.1107/S1600576719010343.

[8] D. Kim *et al.*, “Electric Triggering for Enhanced Control of Droplet Generation,” *Anal. Chem.*, vol. 91, no. 15, pp. 9792–9799, Aug. 2019, doi: 10.1021/acs.analchem.9b01449.

[9] B. Ameduri, R. Bongiovanni, G. Malucelli, A. Pollicino, and A. Priola, “New fluorinated acrylic monomers for the surface modification of UV-curable systems,” *J. Polym. Sci. Part Polym. Chem.*, vol. 37, no. 1, pp. 77–87, 1999, doi: 10.1002/(SICI)1099-0518(19990101)37:1<77::AID-POLA9>3.0.CO;2-0.

[10] R. A. Cirelli, G. P. Watson, and O. Nalamasu, “Optical Lithography,” in *Encyclopedia of Materials: Science and Technology*, Elsevier, 2001, pp. 6441–6448.

[11] B. S. Yilbas, A. Al-Sharafi, and H. Ali, “Surfaces for Self-Cleaning,” in *Self-Cleaning of Surfaces and Water Droplet Mobility*, Elsevier, 2019, pp. 45–98.

[12] F. Fang, S. Aabith, S. Homer-Vanniasinkam, and M. K. Tiwari, “High-resolution 3D printing for healthcare underpinned by small-scale fluidics,” in *3D Printing in Medicine*, Elsevier, 2017, pp. 167–206.

[13] R. Wollhofen, J. Katzmann, C. Hrelescu, J. Jacak, and T. A. Klar, “120 nm resolution and 55 nm structure size in STED-lithography,” *Opt. Express*, vol. 21, no. 9, pp. 10831–10840, May 2013, doi: 10.1364/OE.21.010831.

[14] J. Fischer and M. Wegener, “Three-dimensional optical laser lithography beyond the diffraction limit,” 2013, doi: 10.1002/lpor.201100046.

[15] R. Schwalm, “Photoinitiators and Photopolymerization,” in *Encyclopedia of Materials: Science and Technology*, Elsevier, 2001, pp. 6946–6951.

[16] J. Halling, Ed., *Principles of tribology*, Paperback ed. London: Macmillan, 1978.

[17] S. C. Moldoveanu and V. David, “RP-HPLC Analytical Columns,” in *Selection of the HPLC Method in Chemical Analysis*, Elsevier, 2017, pp. 279–328.

[18] C. Q. Sun, “Differential Phonon Spectrometrics (DPS),” in *Solvation Dynamics*, vol. 121, Singapore: Springer Singapore, 2019, pp. 19–35.

[19] R. S. Hebbar, A. M. Isloor, and A. F. Ismail, “Contact Angle Measurements,” in *Membrane Characterization*, Elsevier, 2017, pp. 219–255.

[20] V. Jokinen and S. Franssila, “Capillarity in microfluidic channels with hydrophilic and hydrophobic walls,” *Microfluid. Nanofluidics*, vol. 5, no. 4, pp. 443–448, Oct. 2008, doi: 10.1007/s10404-008-0263-y.

[21] R. P. Sear, “Specific protein–protein binding in many-component mixtures of proteins,” *Phys. Biol.*, vol. 1, no. 2, pp. 53–60, Jun. 2004, doi: 10.1088/1478-3967/1/2/001.

[22] C. E. Chivers, A. L. Koner, E. D. Lowe, and M. Howarth, “How the biotin–streptavidin interaction was made even stronger: investigation via crystallography and a chimaeric tetramer,” *Biochem. J.*, vol. 435, no. 1, pp. 55–63, Apr. 2011, doi: 10.1042/BJ20101593.

[23] B. Buchegger, S. Mayr, J. Kreutzer, R. Wollhofen, J. Jacak, and T. A. Klar, “Nanostructured Functional Polymers for Selective Protein Binding,” *Biophys. J.*, vol. 112, no. 3, Supplement 1, p. 306a, Feb. 2017, doi: 10.1016/j.bpj.2016.11.1655.

[24] J. C. Foreman, T. Johansen, and A. J. Gibb, Eds., *Textbook of receptor pharmacology*, 3rd ed. Boca Raton, FL: CRC Press, 2011.

[25] J.-F. Masson, T. M. Battaglia, J. Cramer, S. Beaudoin, M. Sierks, and K. S. Booksh, “Reduction of nonspecific protein binding on surface plasmon resonance biosensors,” *Anal. Bioanal. Chem.*, vol. 386, no. 7–8, pp. 1951–1959, Nov. 2006, doi: 10.1007/s00216-006-0834-2.

[26] F. Askari, M. Zandi, P. Shokrolahi, M. H. Tabatabaei, and E. Hajirasoliha, “Reduction in protein absorption on ophthalmic lenses by PEGDA bulk modification of silicone acrylate-based formulation,” *Prog. Biomater.*, vol. 8, no. 3, pp. 169–183, Sep. 2019, doi: 10.1007/s40204-019-00119-x.

[27] M. Rabe, D. Verdes, and S. Seeger, “Understanding protein adsorption phenomena at solid surfaces,” *Adv. Colloid Interface Sci.*, vol. 162, no. 1–2, pp. 87–106, Feb. 2011, doi: 10.1016/j.cis.2010.12.007.

[28] “Pentaerythritol triacrylate 246794,” *3524-68-3*. https://www.sigmaaldrich.com/catalog/product/aldrich/246794 (accessed Apr. 28, 2020).

[29] B. Buchegger *et al.*, “Proteins on Supported Lipid Bilayers Diffusing around Proteins Fixed on Acrylate Anchors,” *Anal. Chem.*, vol. 90, no. 21, pp. 12372–12376, Nov. 2018, doi: 10.1021/acs.analchem.8b02588.

[30] “Poly(ethylene glycol) diacrylate | Sigma-Aldrich.” https://www.sigmaaldrich.com/catalog/substance/polyethyleneglycoldiacrylate123452657048911?lang=en&region=US (accessed Apr. 28, 2020).

[31] D. W. Grainger and C. W. Stewart, “Fluorinated Coatings and Films: Motivation and Significance,” in *Fluorinated Surfaces, Coatings, and Films*, vol. 787, D. G. Castner and D. W. Grainger, Eds. Washington, DC: American Chemical Society, 2001, pp. 1–14.

[32] “2,2,3,3,4,4,5,5,6,6,7,7-<WBR>Dodecafluoroheptyl acrylate 474428,” *Sigma-Aldrich*. https://www.sigmaaldrich.com/catalog/product/aldrich/474428 (accessed Apr. 28, 2020).

[33] “Phenylbis(2,4,6-<WBR>trimethylbenzoyl)<WBR>phosphine oxide 511447,” *BAPOs*. https://www.sigmaaldrich.com/catalog/product/aldrich/511447 (accessed Apr. 28, 2020).

[34] N.-T. Nguyen, “Fabrication technologies,” in *Micromixers*, Elsevier, 2012, pp. 113–161.

[35] F. Deflorian and M. Fedel, “UV-curable organic polymer coatings for corrosion protection of steel,” in *Handbook of Smart Coatings for Materials Protection*, Elsevier, 2014, pp. 530–559.

[36] J. J. Licari and D. W. Swanson, “Chemistry, Formulation, and Properties of Adhesives,” in *Adhesives Technology for Electronic Applications*, Elsevier, 2011, pp. 75–141.

[37] J. Stampfl, R. Liska, and A. Ovsianikov, Eds., *Multiphoton lithography: techniques, materials and applications*. Weinheim: Wiley-VCH Verlag GmbH & Co. KGaA, 2017.

[38] D. P. DePonte *et al.*, “Gas dynamic virtual nozzle for generation of microscopic droplet streams,” *J. Phys. Appl. Phys.*, vol. 41, no. 19, p. 195505, Sep. 2008, doi: 10.1088/0022-3727/41/19/195505.

[39] “Describe.manual.pdf.” Accessed: Apr. 23, 2020. [Online]. Available: https://cmi.epfl.ch/photo/files/Nanoscribe/Describe.manual.pdf.

[40] R. Ahirwar, S. Bariar, A. Balakrishnan, and P. Nahar, “BSA blocking in enzyme-linked immunosorbent assays is a non-mandatory step: a perspective study on mechanism of BSA blocking in common ELISA protocols,” *RSC Adv.*, vol. 5, no. 121, pp. 100077–100083, Nov. 2015, doi: 10.1039/C5RA20750A.

[41] S. Rai, U. Bhardwaj, A. Misra, S. Singh, and R. Gupta, “Comparison between photostability of Alexa Fluor 448 and Alexa Fluor 647 with conventional dyes FITC and APC by flow cytometry,” *Int. J. Lab. Hematol.*, vol. 40, no. 3, pp. e52–e54, Jun. 2018, doi: 10.1111/ijlh.12809.

[42] F. Rost, “Fluorescence Microscopy, Applications,” in *Encyclopedia of Spectroscopy and Spectrometry*, Elsevier, 1999, pp. 565–570.

[43] D. Llères, S. Swift, and A. I. Lamond, “Detecting Protein-Protein Interactions In Vivo with FRET using Multiphoton Fluorescence Lifetime Imaging Microscopy (FLIM),” *Curr. Protoc. Cytom.*, vol. 42, no. 1, Oct. 2007, doi: 10.1002/0471142956.cy1210s42.

[44] J. Ribas Gispert, *Coordination chemistry*. Weinheim: Wiley-VCH, 2008.

[45] "Laser Scanning Microscopy Tutorial," Dec. 02, 2019. https://www.thorlabs.com/newgrouppage9.cfm?objectgroup_id=10765 (accessed Dec. 02, 2019).